Research Article | Vol. 25, No. 13 | 26 Jun 2017 | OPTICS EXPRESS 14134
Optics EXPRESS

Light enhancement by quasi-bound states in the continuum in dielectric arrays

EVGENY N. BULGAKOV[1,2] AND DMITRII N. MAKSIMOV[1,2,*]

[1]*Reshetnev Siberian State University of Science and Technology, 660037, Krasnoyarsk, Russia*
[2]*Kirensky Institute of Physics, Federal Research Center KSC SB RAS, 660036, Krasnoyarsk, Russia*
[*]*mdn@tnp.krasn.ru*

Abstract: The article reports on light enhancement by structural resonances in linear periodic arrays of identical dielectric elements. As the basic elements both subwavelength spheres and rods with circular cross section have been considered. In either case it has been demonstrated numerically that high-*Q* structural resonant modes originated from bound states in the continuum enable near-field amplitude enhancement by factor of 10–25 in the red-to-near infrared range in lossy silicon. The asymptotic behavior of the *Q*-factor with the number of elements in the array is explained theoretically by analyzing quasi-bound states propagation bands.

OCIS codes: (050.1950) Diffraction gratings; (050.6624) Subwavelength structures; (230.5750) Resonators; (290.4210) Multiple scattering; (350.4238) Nanophotonics and photonic crystals.

References and links

1. M. Yu, Y.-Z. Long, B. Sun, and Z. Fan, "Recent advances in solar cells based on one-dimensional nanostructure arrays," Nanoscale **4**, 2783 (2012).
2. M. Burresi, F. Pratesi, F. Riboli, and D. S. Wiersma, "Complex photonic structures for light harvesting," Advanced Optical Materials **3**, 722–743 (2015).
3. P. Sheng, A. N. Bloch, and R. S. Stepleman, "Wavelength-selective absorption enhancement in thin-film solar cells," Appl. Phys. Lett. **43**, 579–587 (1983).
4. C. Heine and R. H. Morf, "Submicrometer gratings for solar energy applications," Appl. Opt. **34**, 2476–2482 (1995).
5. P. Bermel, C. Luo, L. Zeng, L. C. Kimerling, and J. D. Joannopoulos, "Improving thin-film crystalline silicon solar cell efficiencies with photonic crystals," Opt. Express **15**, 16986 (2007).
6. M. Kroll, S. Fahr, C. Helgert, C. Rockstuhl, F. Lederer, and T. Pertsch, "Employing dielectric diffractive structures in solar cells - a numerical study," Physica Status Solidi (a) **205**, 2777–2795 (2008).
7. C. Wang, S. Yu, W. Chen, and C. Sun, "Highly efficient light-trapping structure design inspired by natural evolution," Scientific Reports **3**, 1025 (2013).
8. N. Dhindsa, J. Walia, M. Pathirane, I. Khodadad, W. S. Wong, and S. S. Saini, "Adjustable optical response of amorphous silicon nanowires integrated with thin films," Nanotechnology **27**, 145703 (2016).
9. Z. Yu, A. Raman, and S. Fan, "Fundamental limit of light trapping in grating structures," Opt. Express **18**, A366 (2010).
10. E. Yablonovitch, "Statistical ray optics," J. Opt. Soc. Am. **72**, 899–907 (1982).
11. Z. Yu, A. Raman, and S. Fan, "Nanophotonic light-trapping theory for solar cells," Appl. Phys. A **105**, 329–339 (2011).
12. S. John, "Why trap light?" Nature Materials **11**, 997–999 (2012).
13. G. Bartal, G. Lerosey, and X. Zhang, "Subwavelength dynamic focusing in plasmonic nanostructures using time reversal," Phys. Rev. B **79**, 201103(R) (2009).
14. J. A. Schuller, E. S. Barnard, W. Cai, Y. C. Jun, J. S. White, and M. L. Brongersma, "Plasmonics for extreme light concentration and manipulation," Nature Materials **9**, 193–204 (2010).
15. Z. Fang, Q. Peng, W. Song, F. Hao, J. Wang, P. Nordlander, and X. Zhu, "Plasmonic focusing in symmetry broken nanocorrals," Nano Letters **11**, 893–897 (2011).
16. A. J. Pasquale, B. M. Reinhard, and L. Dal Negro, "Concentric necklace nanolenses for optical near-field focusing and enhancement," ACS Nano **6**, 4341–4348 (2012).
17. J. Zhang, Z. Guo, C. Ge, W. Wang, R. Li, Y. Sun, F. Shen, S. Qu, and J. Gao, "Plasmonic focusing lens based on single-turn nano-pinholes array," Opt. Express **23**, 17883 (2015).
18. T. Y. Jeon, D. J. Kim, S.-G. Park, S.-H. Kim, and D.-H. Kim, "Nanostructured plasmonic substrates for use as sers sensors," Nano Convergence **3**, 18 (2016).
19. A. Zhang and Z. Guo, "Efficient light trapping in tapered silicon nanohole arrays," Optik **127**, 2861–2865 (2016).

#287909 https://doi.org/10.1364/OE.25.014134
Journal © 2017 Received 3 Mar 2017; revised 11 May 2017; accepted 24 May 2017; published 13 Jun 2017

Optics EXPRESS

20. A. Chutinan and S. John, "Light trapping and absorption optimization in certain thin-film photonic crystal architectures," Phys. Rev. A **78**, 023825 (2008).
21. C. Lin and M. L. Povinelli, "Optical absorption enhancement in silicon nanowire arrays with a large lattice constant for photovoltaic applications," Opt. Express **17**, 19371 (2009).
22. K. X. Wang, Z. Yu, V. Liu, A. Raman, Y. Cui, and S. Fan, "Light trapping in photonic crystals," Energy & Environmental Science **7**, 2725 (2014).
23. M. A. K. Othman, F. Yazdi, A. Figotin, and F. Capolino, "Giant gain enhancement in photonic crystals with a degenerate band edge," Phys. Rev. B **93**, 024301 (2016).
24. R. S. Savelev, S. V. Makarov, A. E. Krasnok, and P. A. Belov, "From optical magnetic resonance to dielectric nanophotonics (a review)," Opt. Spectrosc. **119**, 551–568 (2015).
25. S. Jahani and Z. Jacob, "All-dielectric metamaterials," Nature Nanotechnology **11**, 23–36 (2016).
26. M. I. Tribelsky, J.-M. Geffrin, A. Litman, C. Eyraud, and F. Moreno, "Small dielectric spheres with high refractive index as new multifunctional elements for optical devices," Scientific Reports **5**, 12288 (2015).
27. F. Borghese, P. Denti, R. Saija, G. Toscano, and O. I. Sindoni, "Effects of aggregation on the electromagnetic resonance scattering of dielectric spherical objects," Il Nuovo Cimento D **6**, 545–558 (1985).
28. M. P. Ioannidou, N. C. Skaropoulos, and D. P. Chrissoulidis, "Study of interactive scattering by clusters of spheres," J. Opt. Soc. Am. A **12**, 1782–1789 (1995).
29. Y.-l. Xu, "Electromagnetic scattering by an aggregate of spheres," Appl. Opt. **34**, 4573–4588 (1995).
30. O. Merchiers, F. Moreno, F. González, and J. M. Saiz, "Light scattering by an ensemble of interacting dipolar particles with both electric and magnetic polarizabilities," Phys. Rev. A **76**, 043834 (2007).
31. M. S. Wheeler, J. S. Aitchison, and M. Mojahedi, "Coupled magnetic dipole resonances in sub-wavelength dielectric particle clusters," J. Opt. Soc. Am. B **27**, 1083–1091 (2010).
32. A. L. Burin, H. Cao, G. C. Schatz, and M. A. Ratner, "High-quality optical modes in low-dimensional arrays of nanoparticles: application to random lasers," J. Opt. Soc. Am. B **21**, 121–131 (2004).
33. G. S. Blaustein, M. I. Gozman, O. Samoylova, I. Y. Polishchuk, and A. L. Burin, "Guiding optical modes in chains of dielectric particles," Opt. Express **15**, 17380–17391 (2007).
34. M. Gozman, I. Polishchuk, and A. Burin, "Light propagation in linear arrays of spherical particles," Phys. Lett. A **372**, 5250–5253 (2008).
35. A. L. Burin, "Bound whispering gallery modes in circular arrays of dielectric spherical particles," Phys. Rev. E **73**, 066614 (2006).
36. Y. H. Fu, A. I. Kuznetsov, A. E. Miroshnichenko, Y. F. Yu, and B. Luk'yanchuk, "Directional visible light scattering by silicon nanoparticles," Nature Communications **4**, 1527 (2013).
37. U. Zywietz, M. K. Schmidt, A. B. Evlyukhin, C. Reinhardt, J. Aizpurua, and B. N. Chichkov, "Electromagnetic resonances of silicon nanoparticle dimers in the visible," ACS Photonics **2**, 913–920 (2015).
38. P. A. Dmitriev, D. G. Baranov, V. A. Milichko, S. V. Makarov, I. S. Mukhin, A. K. Samusev, A. E. Krasnok, P. A. Belov, and Y. S. Kivshar, "Resonant raman scattering from silicon nanoparticles enhanced by magnetic response," Nanoscale **8**, 9721–9726 (2016).
39. J. Du, S. Liu, Z. Lin, J. Zi, and S. T. Chui, "Dielectric-based extremely-low-loss subwavelength-light transport at the nanoscale: An alternative to surface-plasmon-mediated waveguiding," Phys. Rev. A **83**, 035803 (2011).
40. R. S. Savelev, A. P. Slobozhanyuk, A. E. Miroshnichenko, Y. S. Kivshar, and P. A. Belov, "Subwavelength waveguides composed of dielectric nanoparticles," Phys. Rev. B **89**, 035435 (2014).
41. E. N. Bulgakov and D. N. Maksimov, "Light guiding above the light line in arrays of dielectric nanospheres," Opt. Lett. **41**, 3888–3891 (2016).
42. A. E. Krasnok, A. E. Miroshnichenko, P. A. Belov, and Y. S. Kivshar, "All-dielectric optical nanoantennas," Opt. Express **20**, 20599–20604 (2012).
43. D. S. Filonov, A. P. Slobozhanyuk, A. E. Krasnok, P. A. Belov, E. A. Nenasheva, B. Hopkins, A. E. Miroshnichenko, and Y. S. Kivshar, "Near-field mapping of fano resonances in all-dielectric oligomers," Appl. Phys. Lett. **104**, 021104 (2014).
44. K. E. Chong, B. Hopkins, I. Staude, A. E. Miroshnichenko, J. Dominguez, M. Decker, D. N. Neshev, I. Brener, and Y. S. Kivshar, "Observation of fano resonances in all-dielectric nanoparticle oligomers," Small **10**, 1985–1990 (2014).
45. C. W. Hsu, B. Zhen, A. D. Stone, J. D. Joannopoulos, and M. Soljačić, "Bound states in the continuum," Nature Reviews Materials **1**, 16048 (2016).
46. Y. Plotnik, O. Peleg, F. Dreisow, M. Heinrich, S. Nolte, A. Szameit, and M. Segev, "Experimental observation of optical bound states in the continuum," Phys. Rev. Lett. **107**, 183901 (2011).
47. J. Lee, B. Zhen, S.-L. Chua, W. Qiu, J. D. Joannopoulos, M. Soljačić, and O. Shapira, "Observation and differentiation of unique high-QOptical resonances near zero wave vector in macroscopic photonic crystal slabs," Phys. Rev. Lett. **109**, 067401 (2012).
48. S. Weimann, Y. Xu, R. Keil, A. E. Miroshnichenko, A. Tünnermann, S. Nolte, A. A. Sukhorukov, A. Szameit, and Y. S. Kivshar, "Compact surface fano states embedded in the continuum of waveguide arrays," Phys. Rev. Lett. **111**, 240403 (2013).
49. Chia Wei Hsu, B. Zhen, J. Lee, S.-L. Chua, S. G. Johnson, J. D. Joannopoulos, and M. Soljačić, "Observation of trapped light within the radiation continuum," Nature **499**, 188–191 (2013).

Optics EXPRESS

50. G. Corrielli, G. Della Valle, A. Crespi, R. Osellame, and S. Longhi, "Observation of surface states with algebraic localization," Phys. Rev. Lett. **111**, 220403 (2013).
51. A. Regensburger, M.-A. Miri, C. Bersch, J. Näger, G. Onishchukov, D. N. Christodoulides, and U. Peschel, "Observation of defect states inpt-symmetric optical lattices," Phys. Rev. Lett. **110**, 223902 (2013).
52. E. N. Bulgakov and A. F. Sadreev, "Bloch bound states in the radiation continuum in a periodic array of dielectric rods," Phys. Rev. A **90**, 053801 (2014).
53. L. Yuan and Y. Y. Lu, "Propagating bloch modes above the lightline on a periodic array of cylinders," Journal of Physics B: Atomic, Molecular and Optical Physics **50**, 05LT01 (2016).
54. P.-G. Luan and K.-D. Chang, "Transmission characteristics of finite periodic dielectric waveguides," Opt. Express **14**, 3263–3272 (2006).
55. J. Du, S. Liu, Z. Lin, J. Zi, and S. T. Chui, "Guiding electromagnetic energy below the diffraction limit with dielectric particle arrays," Phys. Rev. A **79**, 205436 (2009).
56. C. S. Kim, A. M. Satanin, Y. S. Joe, and R. M. Cosby, "Resonant tunneling in a quantum waveguide: Effect of a finite-size attractive impurity," Phys. Rev. B **60**, 10962–10970 (1999).
57. S. Venakides and S. P. Shipman, "Resonance and bound states in photonic crystal slabs," SIAM Journal on Applied Mathematics **64**, 322–342 (2003).
58. M. Ladrón de Guevara, F. Claro, and P. Orellana, "Ghost fano resonance in a double quantum dot molecule attached to leads," Phys. Rev. B **67**, 195335 (2003).
59. S. Hein, W. Koch, and L. Nannen, "Trapped modes and fano resonances in two-dimensional acoustical duct-cavity systems," J. Fluid Mech. **692**, 257–287 (2012).
60. S. Zou, N. Janel, and G. C. Schatz, "Silver nanoparticle array structures that produce remarkably narrow plasmon lineshapes," J. Chem. Phys. **120**, 10871–10875 (2004).
61. J. M. Foley, S. M. Young, and J. D. Phillips, "Symmetry-protected mode coupling near normal incidence for narrow-band transmission filtering in a dielectric grating," Phys. Rev. B **89**, 165111 (2014).
62. J. M. Foley and J. D. Phillips, "Normal incidence narrowband transmission filtering capabilities using symmetry-protected modes of a subwavelength, dielectric grating," Opt. Lett. **40**, 2637 (2015).
63. X. Cui, H. Tian, Y. Du, G. Shi, and Z. Zhou, "Normal incidence filters using symmetry-protected modes in dielectric subwavelength gratings," Scientific Reports **6**, 36066 (2016).
64. E. N. Bulgakov and A. F. Sadreev, "Light trapping above the light cone in a one-dimensional array of dielectric spheres," Phys. Rev. A **92**, 023816 (2015).
65. R. A. Shore and A. D. Yaghjian, "Traveling electromagnetic waves on linear periodic arrays of small lossless penetrable spheres," Tech. rep., DTIC Document (2004).
66. C. Linton, V. Zalipaev, and I. Thompson, "Electromagnetic guided waves on linear arrays of spheres," Wave Motion **50**, 29–40 (2013).
67. E. N. Bulgakov and A. F. Sadreev, "Transfer of spin angular momentum of an incident wave into orbital angular momentum of the bound states in the continuum in an array of dielectric spheres," Phys. Rev. A **94**, 033856 (2016).
68. E. Bulgakov and A. Sadreev, "Trapping of light with angular orbital momentum above the light cone," Advanced Electromagnetics **6**, 1 (2017).
69. S. Romano, I. Rendina, and V. Mocella, "High field enhancement factors in photonic nanostructures," in "2015 AEIT International Annual Conference (AEIT)," (2015).
70. V. Mocella and S. Romano, "Giant field enhancement in photonic resonant lattices," Phys. Rev. B **92**, 155117 (2015).
71. J. W. Yoon, S. H. Song, and R. Magnusson, "Critical field enhancement of asymptotic optical bound states in the continuum," Scientific Reports **5**, 18301 (2015).
72. M. G. Silveirinha, "Trapping light in open plasmonic nanostructures," Phys. Rev. A **89**, 023813 (2014).
73. A. Yamilov and H. Cao, "Density of resonant states and a manifestation of photonic band structure in small clusters of spherical particles," Phys. Rev. B **68**, 085111 (2003).
74. K. Yasumoto, *Electromagnetic theory and applications for photonic crystals* (CRC Press, 2005).
75. X. Gao, C. W. Hsu, B. Zhen, X. Lin, J. D. Joannopoulos, M. Soljačić, and H. Chen, "Formation mechanism of guided resonances and bound states in the continuum in photonic crystal slabs," Scientific Reports **6**, 31908 (2016).
76. L. Yuan and Y. Y. Lu, "Strong resonances on periodic arrays of cylinders and optical bistability with weak incident waves," Phys. Rev. A **95**, 023834 (2017).
77. J. A. Stratton, *Electromagnetic theory* (McGraw-Hill Book Company, Inc., 1941).
78. G. Vuye, S. Fisson, V. Nguyen Van, Y. Wang, J. Rivory, and F. AbelÃĺs, "Temperature dependence of the dielectric function of silicon using in situ spectroscopic ellipsometry," Thin Solid Films **233**, 166–170 (1993).
79. M. A. Green and M. J. Keevers, "Optical properties of intrinsic silicon at 300 K," Progress in Photovoltaics: Research and Applications **3**, 189–192 (1995).
80. P. Velha, E. Picard, T. Charvolin, E. Hadji, J. Rodier, P. Lalanne, and D. Peyrade, "Ultra-high Q/V Fabry-Perot microcavity on SOI substrate," Opt. Express **15**, 16090 (2007).
81. W. Suh, Z. Wang, and S. Fan, "Temporal coupled-mode theory and the presence of non-orthogonal modes in lossless multimode cavities," IEEE J. Quantum Electron. **40**, 1511–1518 (2004).
82. A. Kodigala, T. Lepetit, Q. Gu, B. Bahari, Y. Fainman, and B. Kanté, "Lasing action from photonic bound states in continuum," Nature **541**, 196–199 (2017).

Optics EXPRESS

83. L. Ni, J. Jin, C. Peng, and Z. Li, "Analytical and statistical investigation on structural fluctuations induced radiation in photonic crystal slabs," Opt. Express **25**, 5580–5593 (2017).
84. Z. F. Sadrieva, I. S. Sinev, K. L. Koshelev, A. Samusev, I. V. Iorsh, O. Takayama, R. Malureanu, A. A. Bogdanov, and A. V. Lavrinenko, "Transition from optical bound states in the continuum to leaky resonances: Role of substrate and roughness," ACS Photonics **4**, 723–727 (2017).
85. M. Rybin and Y. Kivshar, "Optical physics: Supercavity lasing," Nature **541**, 164–165 (2017).

1. Introduction

Light trapping by periodic structures is a mainstream idea in thin film photovoltaics [1, 2]. The idea dates back to the paper by Sheng, Bloch, and Steplemann who fist proposed to employ a periodic grating substrate in amorphous silicon solar cells [3]. Since then the periodic structures that diffract light and increase the optical length within the absorbing material have been a subject of numerous publications [4–8]. Most remarkably the dielectric gratings have allowed for large enhancement factors [9] which exceed the fundamental limit for a Lambertian cell [10] that holds well only if there is a high density of optical modes in the plane of the structure. At the same time as one approaches the nanophotonic regime the wave nature of light comes into play to call for theoretical approaches taking into account optical resonances [11].

Due to numerous applications [12] trapping, focusing, and concentration of light at the nanoscale have recently emerged as topics of great interest primarily in regard to various plasmonic devices [13–19] and photonic band-gap structures [20–23]. Another promising directions of research is all-dielectric nanophotonics [24, 25] which employs subwavelength dielectric objects, such as e.g. spherical nanoparticles [26], to tailor the resonant response of the system. Scattering by clusters dielectric spheres has been in research focus for a long time [27–31] with high-Q resonant modes in linear [32–34] as well as circular [35] arrays predicted a decade ago. Nowadays, thanks to immense progress in manipulating dielectric nanoparticles [36–38], we witness a surge of interest in optical devices based on clusters and arrays of dielectric spheres including subwavelength waveguides [39–41], optical nanoantenas [36, 42], and circular oligomers [43, 44].

In this article we consider light enhancement by high-Q structural resonances in linear one-dimensional periodic arrays of identical dielectric elements. In what follows the term *structural resonance* will be applied to a resonance whose position and width are dictated by the spatial distribution of dielectric elements. Thus, the structural resonances can be contrasted to both natural material resonances and Mie resonances of individual dielectric elements. As the basic elements both spheres and rods with circular cross section will be considered. To achieve high-Q resonances and, consequently, high enhancement factors we propose to tune the parameters of the arrays to bound states in the continuum (BSCs) which are localized states with the eigenfrequency embedded into continuum of propagating solutions [45]. With the state of the art in the BSC research thoroughly reviewed in the above reference here we simply mention the key experiments on optical BSCs in periodic dielectric structures [46–51].

The BSCs in linear periodic arrays of dielectric cylinders were predicted theoretically in the earlier paper [52] where the role of the BSCs in wave scattering was also highlighted. More recently, the problem of BSCs in arrays of dielectric rods [53] was revisited with the existence domains in the plane of radius and dielectric constant of the cylinders determined through extensive numerical sumulations. Unlike the guided solution below the line of light [54, 55] the qusi-bound modes in the parametric vicinity of a true BSC are resonantly coupled with the freely propagating plane waves to emerge in the scattering cross-section as sharp Fano resonances. In fact the collapse of a Fano resonance is a generic feature inherent to BSCs [56–59] including quasi-BSCs in plasmonics [60]. In the field of optics the above feature has allowed for design of narrow band normal incidence filters [61–63]. The BSCs in linear arrays of dielectric spheres were first reported in [64]. As before for arrays of cylinders we contrast the BSCs in arrays

Optics EXPRESS

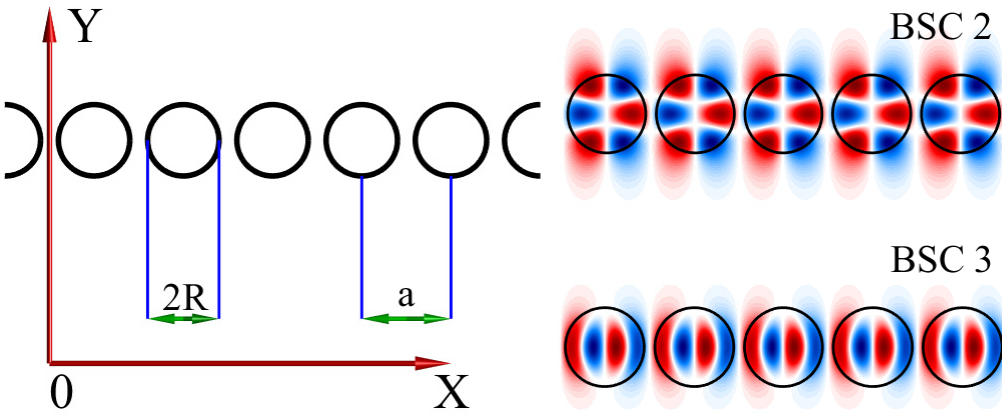

Fig. 1. BCSs in arrays of dielectric rods. Left panel: set-up of the array in $x0y$-plane. Right panel: field patterns of *BSCs* 2, 3 from Table 1.

of spheres to the guided solutions below the line of light [32, 33, 39, 40, 65, 66]. The effect of BSCs on plane wave scattering was considered [67, 68] with the trapping of light with orbital angular momentum theoretically predicted. Light enhancement by symmetry protected BSCs in photonic crystal slab was demonstrated in [69–71]. Here, along the same line we propose to employ arrays of *finite* number of dielectric elements. Although formally BSCs do not exist in finite structures [72] their traces could be observed in form of high-Q structural resonances [41] similarly to the traces of photonic band structure emerging in scattering on small clusters of spherical particles [73].

The article is organized as follows. In Section 2 we briefly review the BSCs in infinite arrays in dielectric rods. Then we demonstrate structural resonances in the parametric vicinity of BSCs in finite arrays. A simple theory predicting the positions of the structural resonances is proposed. In Section 3 we show that the same theory applies for the arrays of dielectric spheres. In Section 4 we elaborate asymptotic behavior of the Q-factor and the enhancement factor for various types of the structural resonances with the increasing number of elements in the array. Finally, we conclude in Section 5.

2. Quasi-BSCs in arrays of dielectric rods

We consider an array of identical dielectric rods of radius R arranged along the x-axis with period a. The axes of the rods are collinear and aligned with the z-axis. The cross-section of the array in $x0y$-plane is shown in Fig. 1 (left panel). The numerical procedure for finding electromagnetic field in arrays of rods is well-known in literature [74] and was adapted for BSCs in [52]. Suppose that the array is illuminated by a stationary TM plane wave with its electric vector pointing along the axes of the rods, then according to the above references we have the scattered field inside the rods in the following form

$$E_z(x,y) = \sum_j \sum_{m=0}^{\infty} c_m(j) e^{im\theta_j} J_m(k_0\sqrt{\epsilon}\rho_j), \tag{1}$$

where j enumerates the rods, θ_j, ρ_j are the local polar coordinates for the j rod, $J_m(k_0\sqrt{\epsilon}\rho_j)$ - the Bessel function, ϵ - the dielectric permittivity, $c_m(j)$ - the expansion coefficient, and k_0 -

Optics EXPRESS

Table 1. BSCs in linear arrays of dielectric cylinders, $\epsilon = 15$. SP stands for symmetry protected.

BSC	SP	$k_0 a$	$k_x^0 a$	R/a	ν	μ	a_ν	a_μ
1	Yes	1.8412	0	0.4400	4	2	$5.25 \cdot 10^{-4}$	0.20
2	Yes	3.0758	0	0.4400	2	2	$9.6 \cdot 10^{-3}$	0.05
3	Yes	3.5553	0	0.4400	4	2	$2.4 \cdot 10^{-3}$	0.177
4	Yes	2.3864	0	0.4400	2	2	$6.85 \cdot 10^{-3}$	0.092
5	No	2.8299	0	0.4441	4	2	$3.17 \cdot 10^{-3}$	-0.085
6	No	3.7156	1.6501	0.4400	2	1	$5.27 \cdot 10^{-3}$	-0.0721

the frequency. Outside the rods we have a similar expression for the scattering function

$$E_z(x,y) = \sum_j \sum_{m=0}^{\infty} \overline{c}_m(j) e^{im\theta_j} H_m^{(1)}(k_0 \rho_j), \tag{2}$$

where $H_m^{(1)}(k_0\rho_j)$ is the outgoing Hankel function. The summation over m in Eqs. (1) and (2) runs to infinity. The only approximation in the numerical method is truncation to a finite number of summands in Eqs. (1) and (2). This approximation makes possible to produce a finite interaction matrix of the scattering system and subsequently a finite number of equations for $c_m(j), \overline{c}_m(j)$ as described in [52]. The method is known to converge rapidly with the number of multipoles [74]. In our computations we used $m = 0, 1, ..., 9$ which results in the relative truncation error 10^{-5} as defined in [41]. We refer the reader to [52] for the lengthy equations for amplitudes $c_m(j), \overline{c}_m(j)$.

2.1. BSCs in infinite arrays

In case of infinite arrays the summation over index j in Eqs. (1) and (2) is run from minus to plus infinity. The translation invariance allows to apply the Bloch theorem in the form [74]

$$c_m(j) = c_m(0) e^{ik_x a j}, \ \overline{c}_m(j) = \overline{c}_m(0) e^{ik_x a j}, \tag{3}$$

where k_x is the x-axis component of the wave vector (Bloch vector). Although the solution (2) is a superposition of outgoing functions it still can be totally decoupled from the far field outgoing waves due to destructive interference between the waves emanating from different rods [52]. In that situation a BSC exists in the system even without the array being illuminated from the far zone. In dependence on k_x the BSCs are exceptional points in the quasi-BSCs propagation bands where the imaginary part of the resonant frequency k_0 turns to zero [41]. In general the asymptotic behavior of the imaginary and real parts of the resonant frequency in the vicinity of a BSCs is described by the following formulas

$$-\Im\{k_0 a\} = a_\nu (k_x a - k_x^{BSC} a)^\nu + O[(k_x a - k_x^{BSC} a)^{\nu+2}], \tag{4}$$

and

$$\Re\{k_0 a\} = k_0^{BSC} a - a_\mu (k_x a - k_x^{BSC} a)^\mu + O[(k_x a - k_x^{BSC} a)^{\mu+1}], \tag{5}$$

where k_0^{BSC} is the BSC frequency, k_x^{BSC} - the BSC wave vector along the array axis, and ν, μ - the leading coefficient of polynomial expansion [41]. The physical meaning of Eq. (4) is simple; once the system is detuned in k_x-space from a true BSC point k_x^{BSC} the resonance acquires finite life-time given by the inverse of $\Im\{k_0\}$. Although the majority of BSCs have $k_x^{BSC} = 0$, there are also so-called Bloch BSCs which are trapped waves travelling along the array [52, 64, 75].

Optics EXPRESS

In Table 1 we collect the parameters of six BSCs found for infinite arrays with $\epsilon = 15$ (Silicon). The values of a_μ and a_ν in Table 1 were extracted from the data by a polynomial fit. For a typical picture of the band structure of Bloch BSCs the reader is addressed to [41].

There are two generic types of BSCs in arrays of dielectric rods [52], symmetry protected, and unprotected by symmetry. Field patterns of symmetry protected *BSCs* 2, 3 are shown in the left panel in Fig. 1 where one can see that those BCSs are symmetrically mismatched with a plane wave normally incident to the array. The asymptotic behavior of the resonance live-times in the vicinity of a BSC was recently considered by Yuan and Lu [76] who argued that for symmetry protected BSCs the leading term should be $\nu = 2$. There were no, however, reliable estimate for $a_{\nu=2}$. In our numerical simulations we found that both $\nu = 2$ and $\nu = 4$ are possible. In Table 1 we presented the data on four symmetry protected BCSs a couple for each $\nu = 2$ and $\nu = 4$. The asymptotic behavior of unprotected BSCs was also considered in [76] with a mathematically rigorous result that for the the standing wave BSCs unprotected by symmetry the leading term is $\nu = 4$ which is in accordance with our findings for *BSC* 5. For Bloch *BSC* 6 we found $\nu = 2$.

2.2. Quasi-BSCs in finite arrays

Next we discuss the the light scattering by various types of quasi-BSCs in finite arrays to highlight the features related to the asymptotic behavior described by Eqs. (4) and (5). The array now consists of N elements and summation over j in Eqs. (1) and (2) runs from 1 to N. In Fig. 2 we present the results of numerical simulations of wave scattering by finite arrays of $N = 50$ rods. The parameters k_0, k_x which are the frequency and the x-component of an impinging TM plane wave were swept in the parametric vicinity of *BSCs* 2 and 3. Notice that only positive k_x were considered for the system is symmetric with respect to the inversion of the x-axis. For simplicity the response was recorded as the mean of the absolute value of the leading coefficient in the expansion Eq. (1)

$$\langle |c_{m_0}| \rangle = \frac{1}{N} \sum_{j=1}^{N} |c_{m_0}(j)|, \tag{6}$$

where m_0 is the index of the coefficients $c_{m_0}(j)$ in Eq. (1) with the largest absolute value (see top panel in Fig. 2 where $m_0 = 1$).

In both cases one can see "bright" spots following the asymptotic expression for the real part of the resonant frequency (5). These spots correspond to the structural resonances with the widths of the spots along k_0-axis proportional to the inverse Q-factors which will be considered in Section 4. The nature of the structural resonances could be easily understood by close examination of the upper panel in Fig. 2 where we plotted the expansion coefficients $c_m(j)$ for the first resonant spot. One can see from the upper panel in Fig. 2 that the solution is nothing but a sinusoidal standing wave locked between the edges of the array. Thus, to recover the spectrum of the structural resonances one can write down the following condition for the $k_x^{(p)}$ of the p structural resonance.

$$N a k_x^{(p)} = \pi p, \ p = 1, 2, \ldots, . \tag{7}$$

Then by virtue of Eq. (5) we have

$$\Re\{k_0^{(p)} a\} = k_0^{BSC} a - a_\mu \left(\frac{\pi p}{N} - k_x^{BSC} a \right)^\mu, \tag{8}$$

with p corresponding to the number of half-wavelengths between the edges and the field patterns

$$E_z^{(p)}(x) \simeq f(x, y) \sin\left(\frac{\pi p x}{N a} \right), \tag{9}$$

Optics EXPRESS

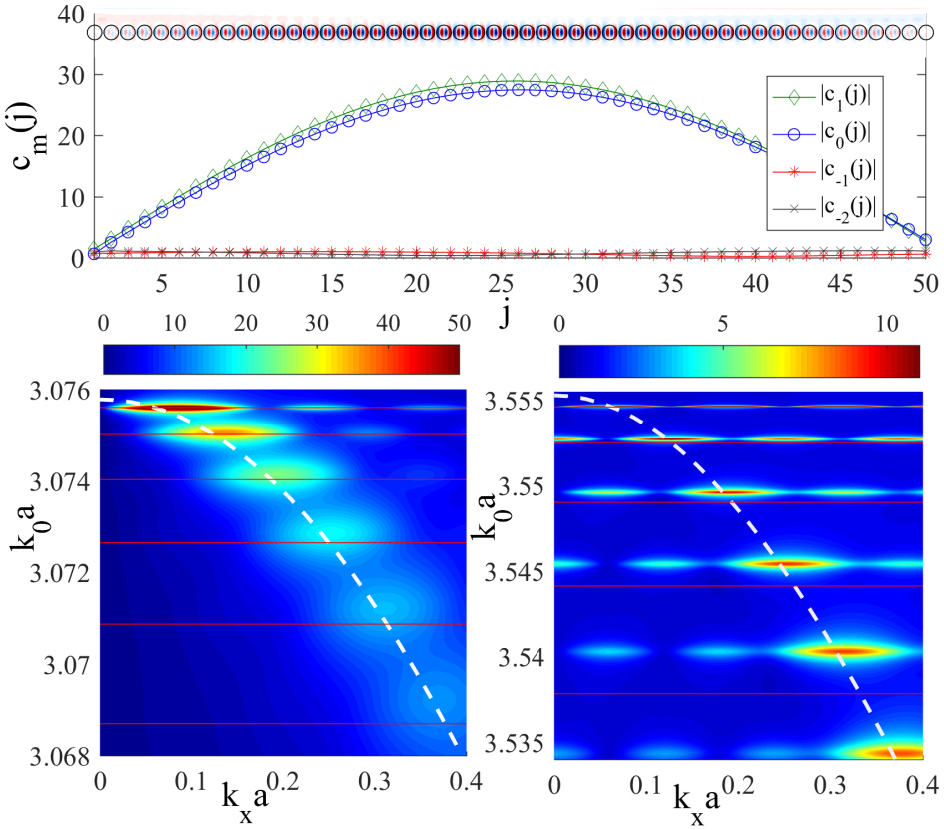

Fig. 2. Light scattering in the parametric vicinity of symmetry protected BSCs for dielectric $\epsilon = 15$ arrays of rods under illumination by a TM plane wave with unit amplitude. Top panel: expansion coefficients $c_m(j)$ vs. the number of the rod j for $N = 50$ for *BSC* 3. The impinging wave parameters are tuned to the first resonance Eq. (7). The resulting field pattern is shown on top of the subplot. South-west: mean value of the leading coefficient $\langle c_{m_0} \rangle$ vs. k_0, k_x in the vicinity of *BSC* 2 for $N = 50$. South-east: The same for *BSC* 3. White dash lines correspond to asymptotic behavior by Eq. (5). The frequencies of structural resonances by Eq. (8) are shown by red horizontal lines.

where $f(x, y) = f(x + a, y)$ is the periodic functions corresponding to the BSCs profiles in Fig. 1. Remarkably, despite the BCSs are standing waves the position of the first structural resonance $p = 1$ is shifted from $k_x = 0$ according to Eqs. (7) and (8). The field pattern of the first resonance is shown on top of the upper panel in Fig. 2 to visualize Eq. (9). Notice the resemblance with *BSC* 3 in Fig. 1. The resonant frequencies by Eq. (8) are plotted in Fig. 2 by red horizontal lines. One can see that Eq. (8) predicts to a good accuracy the positions of two first resonances $p = 1, 2$. For $p \geq 3$ the positions of resonances deviate from Eq. (8) due to the higher order terms in the polynomial expansion Eq. (5). This effect could be eliminated by further increase of the length of the array Na with all resonances shifting to the BSC point according to Eq. (8). In addition to the main sequence (8) in Fig. 2 one can see satellite resonant peaks. We speculate that the satellites are due to oscillating coupling of the structural resonances to the impinging wave with the same frequency but a different k_x component. Finally, one can see from Fig. 2 that a BSC with $\nu = 4$ produces a picture of resonances with smaller high-intensity spots to evidence higher Q-factors.

Optics EXPRESS

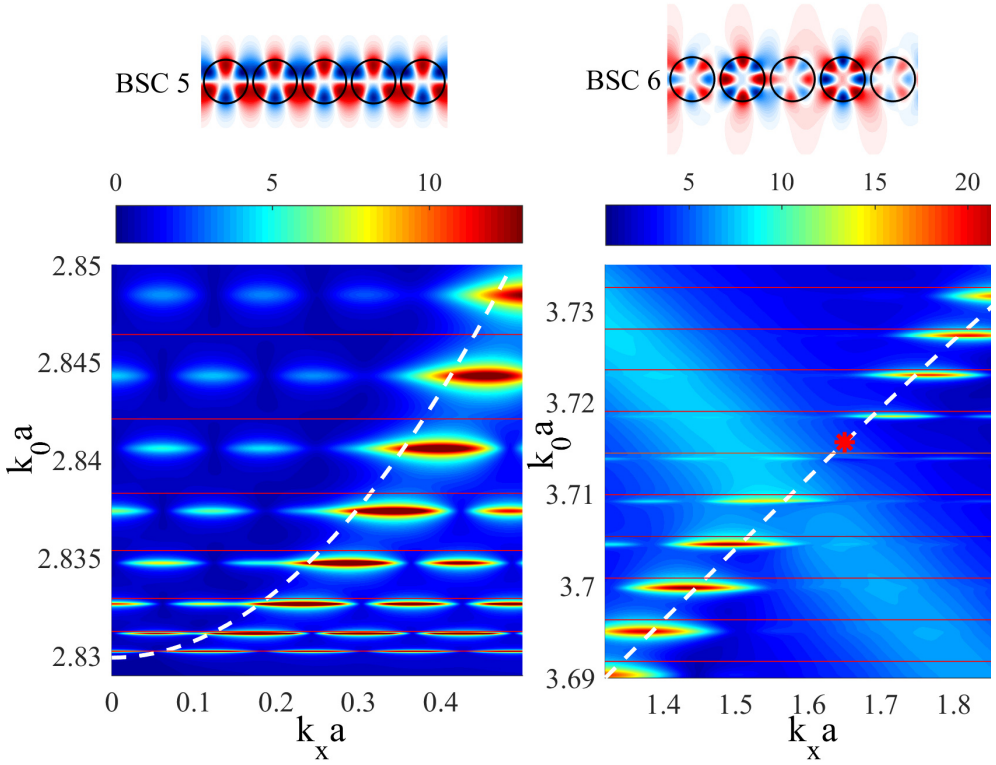

Fig. 3. Light scattering in the parametric vicinity of BSCs unprotected by symmetry for dielectric $\epsilon = 15$ arrays of rods under illumination by a TM plane wave with unit amplitude. Left panel: Standing wave *BSC* 5 unprotected by symmetry; mean value of the leading coefficient $\langle c_{m_0} \rangle$ Eq. (6) vs. k_0, k_x in the parametric vicinity of the BSC for $N = 50$ rods. The BSC field pattern is shown on top of the subplot. Right panel: the same for Bloch *BSC* 6; the star shows the position of *BSC* 6 in the parametric space k_0, k_x. The BSC field pattern is shown on top of the subplot in form of the real part of the travelling wave amplitude. White dash lines correspond to asymptotic behavior by Eq. (5). The frequencies of structural resonances by Eq. (8) are shown by red horizontal lines.

In Fig. 3 we present the results of numerical simulations of wave scattering by finite arrays of N rods in the parametric vicinity of *BSCs* 5 and 6 from Table 1. The field patterns are shown on top of the plot to demonstrate that now the BCSs are not symmetrically mismatched to the normally incident wave. In contrast to symmetry protected ones the BSCs of this sort are much more difficult to come by for they always require some adjustment of either radius R or Bloch vector k_x to occur through an involved interference picture [52]. One can see from Fig. 3 that the response function (6) demonstrates features very similar to those in Fig. 2 with structural resonances emerging at frequencies by Eq. (8). Again for standing wave *BSC* 5 we see that only position of two first structural resonances are accurately predicted by Eq. (8). Another source of error could be additional phase accumulated in reflection from the edge of the array not accounted for by Eq. (7). Also notice that for Bloch *BSC* 6 the structural resonances are equidistant with $a_{\mu=1}$ being the group velocity according to Eq. (5).

Optics EXPRESS

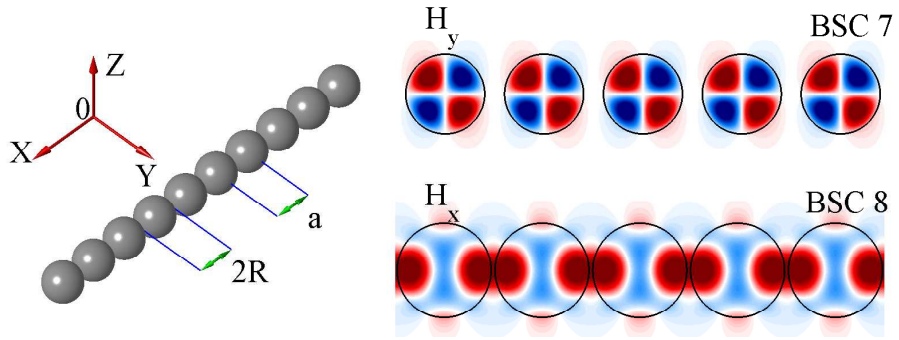

Fig. 4. BCS in arrays of dielectric spheres. Left panel: set-up of the array. Right panel: The field patterns in form of H_y component for *BSC* 7 and H_x component for *BSC* 8 in $x0z$-plane.

Table 2. BSCs in linear arrays of dielectric spheres, $\epsilon = 15$. SP stands for symmetry protected.

BSC	SP	$k_0 a$	$k_x^0 a$	R/a	ν	μ	a_ν	a_μ
7	Yes	3.6022	0	0.400	2	2	$1.366 \cdot 10^{-2}$	0.010
8	No	2.9280	0	0.485	4	2	$0.1818 \cdot 10^{-2}$	-0.0793

3. Quasi-BSCs in arrays of dielectric spheres

The system under scrutiny is schematically depicted in Fig. 4. For arrays dielectric spheres we will follow the recipes from [64] where the method by Linton, Zalipaev, and Thompson [66] was adapted for finding BSCs. The parameters of two BSCs, one symmetry protected, and one unprotected by symmetry are given in Table 2. In the above referenced method the magnetic and electric vectors could be found in terms of Mie coefficients $a_n^m(j), b_n^m(j)$. For instance, outside the spheres one has for the the scattered EM field electric vector $\mathbf{E}(\mathbf{r})$

$$\mathbf{E}(\mathbf{r}) = \sum_j \sum_{n=m^*}^{\infty} \left[a_n^m(j)\mathbf{M}_n^m(\mathbf{r}-\mathbf{r}_j) + b_n^m(j)\mathbf{N}_n^m(\mathbf{r}-\mathbf{r}_j) \right], \tag{10}$$

where j the number of the sphere in the array, $\mathbf{r}_j$ - the coordinates of the j sphere, m - azimuthal number, $m^* = max(1, m)$, and $\mathbf{N}_n^m(\mathbf{r}), \mathbf{M}_n^m(\mathbf{r})$ are spherical vector harmonics [77]. Again in the case of infinite arrays we have according to the Bloch theorem

$$a_n^m(j) = a_n^m(0)e^{ik_x aj}, \; b_n^m(j) = b_n^m(0)e^{ik_x aj}. \tag{11}$$

In this paper we restrict ourself we with $m = 0$, though BSCs with higher orbital angular momentum are possible [67, 68]. The field patterns of BSCs from Table 2 are shown in the left panel in Fig. 4. Notice that *BSC* 7 in Table 2 is a wave of the TM-type which means H_x=0, and $b_n^0(j) = 0$ [64]. In contrast *BSC* 8 is a TE-wave with E_x=0, and $b_n^0(j) = 0$.

Let us now consider the resonant response of finite array with N spheres. Despite the similarity of Eq. (10) to Eqs. (1) and (2) the numerical method is now computationally much more expensive due to the necessity to evaluate lattice sums with involved special functions [66]. Though limited to the power of a desktop computer we can still circumvent the computational difficulties by recollecting the resonant picture from the previous section. First by using Eq. (8) one can obtain the frequencies of a structural resonance. Then the response function Eq. (6) is

Optics EXPRESS

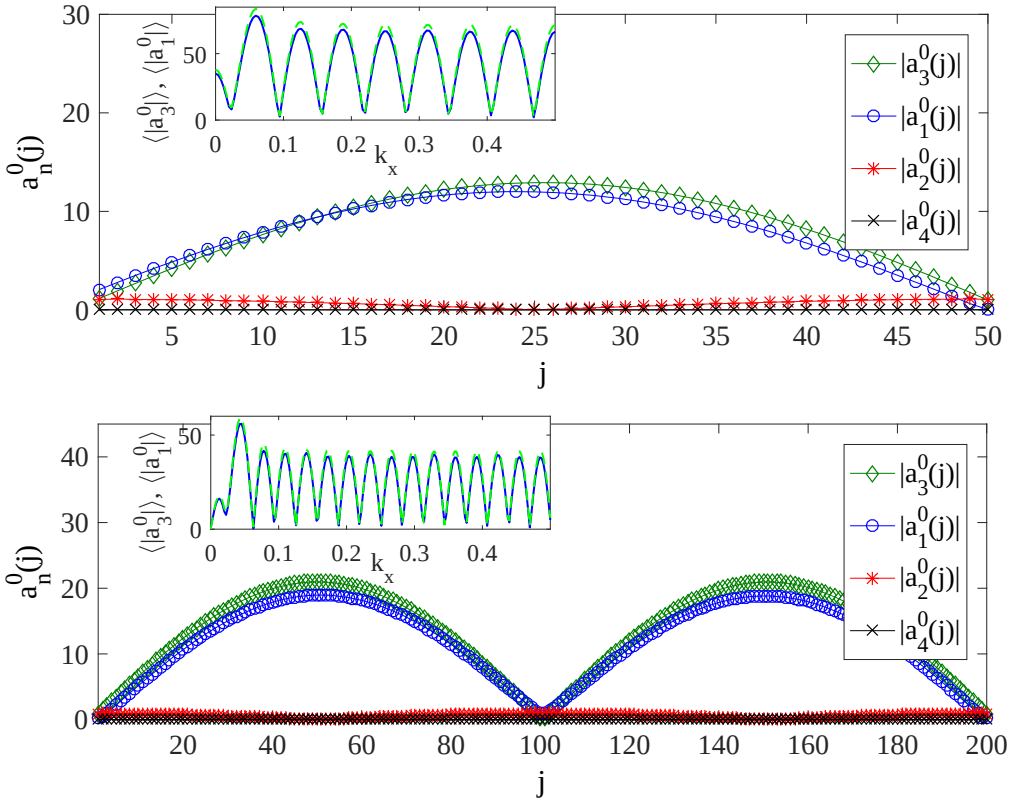

Fig. 5. Light scattering by structural resonances in the parametric vicinity of *BSC* 8 in arrays of dielectric spheres. Top panel: the leading coefficients in Eq. (10) for the first structural resonance $N = 50$. Bottom panel: the leading coefficients in Eq. (10) for the second structural resonance $N = 200$. The insets show the response function Eq. (6) evaluated with leading Mie coefficients $a_1^0(j), a_3^0(j)$ against the Bloch wave vector k_x.

computed numerically only in dependance on k_x with coefficients $a_n^0(j), b_n^0(j)$ from Eq. (10) now used instead of $c_m(j)$ in Eq. (6). The results for *BSC* 8 from Table 2 under illumination by a TE-polarized plane wave of unit amplitude are plotted in Fig. 5. Again one can see sinusoidal standing waves similar to Fig. 2. Notice that for the second resonance $p = 2$ in Eq. (8) we intentionally chose $N = 200$ to eliminated the errors due to the higher order terms in Eq. (5). The response function against k_x for k_0 corresponding to the first and the second resonances Eq. (8) is also demonstrated in the insets in Fig. 5. Again one observes an oscillatory dependance with a pronounced maximum corresponding to Eq. (7) as in Figs. 2,3. For *BSC* 7 the same results were observed under illumination by a TM-polarized plane wave.

4. Light enhancement

Bearing in mind the structure of resonant response of finite arrays we can now address the question of how many dielectric elements in the array are needed to observe the effect of light enhancement in a realistic experiment with two figures of merit being the quality and enhancement factors. Before proceeding to the assessment of those quantities we would like to mention that so far all results were presented in dimensionless units to emphasize that the model is applicable to silicon dielectric arrays both in the visible as well as in the near infrared where the real part of the dielectric constant varies insignificantly with the frequency of light [78, 79].

Optics EXPRESS

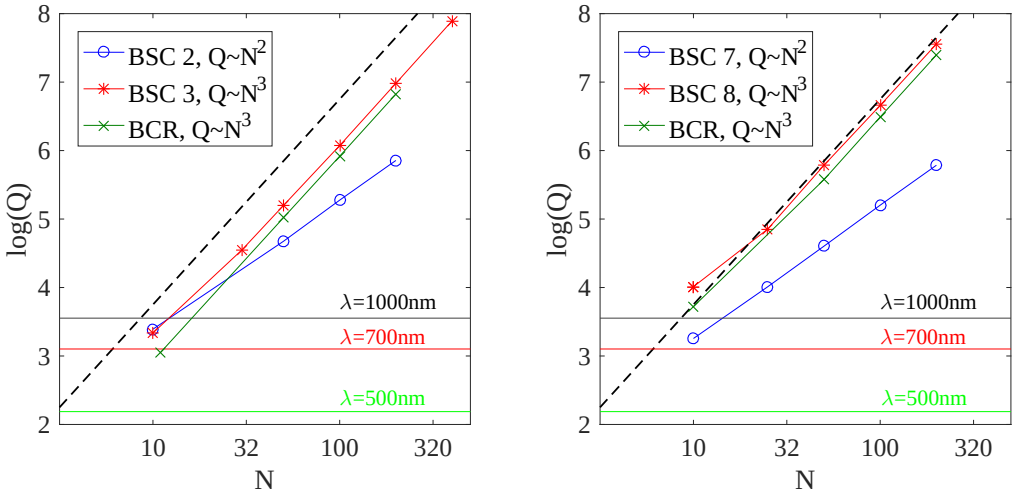

Fig. 6. Q-factors for structural resonances against the number of dielectric elements N. Left panel: arrays of rods; BCR with $k_0 a = 2.8908, k_x a = \pi, R/a = 0.44$. Right panel: arrays of spheres; BCR with $k_0 a = 2.052, k_x a = \pi, R/a = 0.40$. The black dash line shows the best result found in [33]. The horizontal lines show the limits due to material losses in silicon.

It should be noted, however, that the imaginary part in the same range can vary by orders of magnitude. Thus, one may expect that the effect of light enhancement will be limited by the material losses in silicon.

4.1. *Q-factors*

Here we use the standard definition of the Q-factor

$$Q = \frac{\omega}{\gamma}, \tag{12}$$

where ω is the resonance frequency, and γ is the resonance width, both quantities extracted from the scattering data described in the previous sections Figs. 2,5. The Q-factors against the number of dielectric elements in the array for the first ($p = 1$ in Eq. (8)) structural resonance of *BSCs* $2, 3, 7$, and 8 are plotted in Fig. 6. As expected from Eqs. (4) and (7) the Q-factor for resonances with $\nu = 2$ scales as $Q \sim N^2$, however, for $\nu = 4$ we observed $Q \sim N^3$ which, seemingly, contradicts our theoretical predictions. The contradiction can be resolved by noticing that Eq. (4) only describes one specific mechanism of the radiation losses equally applicable for both finite and infinite arrays, namely, the radiation from the sides of the arrays due to detuning from the true BSC point in the parametric space. In the case of finite arrays there is another radiation mechanism due to the losses at the edges as the wave bounces between them to form the sinusoidal resonant mode shape Eq. (9). Obviously, for the guided modes below the line of light that would be the only possible radiation mechanism because the radiative losses at the sides are forbidden by total internal reflection. In fact, the scaling law for the edge radiation is already obtained in [33] where the authors demonstrated that the Q-factor scales as $Q \sim N^3$. Thus, one can conclude that in case of $\nu = 4$ the radiative losses at the sides are suppressed by the radiative losses at the edges resulting in the scaling law for resonances formed by guided modes below the line of light [33].

In accordance with our findings we can now define *side-coupled resonances* with $Q \sim N^2$ for BSCs with $\nu = 2$, and a wider class of *edge-coupled resonances* with $Q \sim N^3$ which

Optics EXPRESS

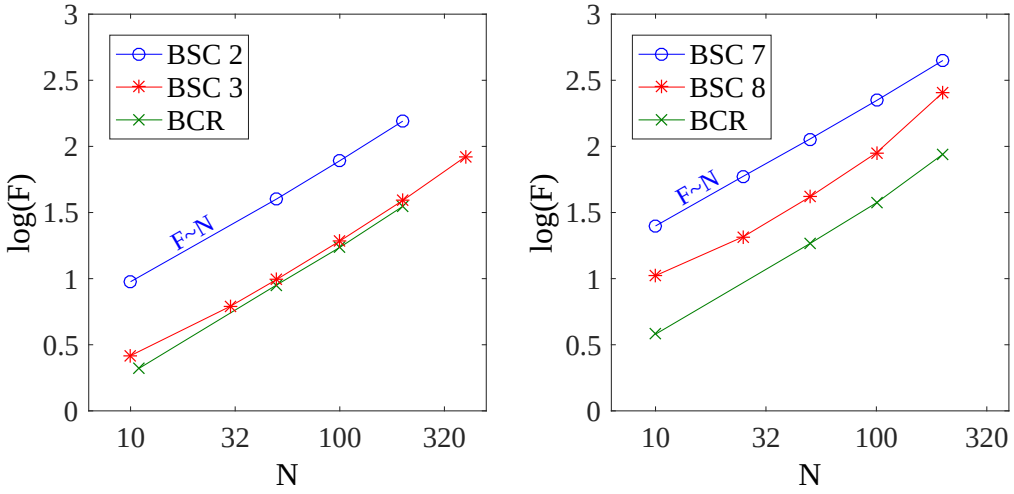

Fig. 7. The enhancement factor of dielectric arrays. Left panel: arrays of rods. Right panel: arrays of spheres.

encompasses both BSCs with $\nu = 4$ as well as the below continuum resonances (BCRs). Now it is instructive to compare our results with the Q-factors for the BCRs. To do that in Fig. 6 we plot the Q-factors for two BCR one for rods and spheres each. The parameters of the BCRs are given in the caption to Fig. 6. One can see that both $\nu = 2$ BSCs and BCR demonstrate a similar dependance against N.

Finally, let us access the role of the material losses. The Q-factor limits were estimated based on the data on the imaginary part of refractive index at $\lambda = 500, 700$nm by [78], and at $\lambda =$ 1000nm by [79]. One can easily see from Fig. 6 that $Q \approx 10^3$–10^4 resonances can be observed with silicon in the red-to-near-infrared range for arrays of $N \approx 10$–15 elements.

4.2. Enhancement factors

We define the enhancement factor F as the average of the square root of the field intensity $I(\mathbf{r})$ within the volume $V = \pi R^2 N a$ (or area $2RNa$) containing the whole of the finite array divided by the square root of the field intensity carried by the incoming wave I_0.

$$F = \frac{1}{\sqrt{I_0} V} \int_V d\mathbf{r} \sqrt{I(\mathbf{r})}. \tag{13}$$

Although according to Eq. (9) the EM-field varies significantly in the vicinity of the array the enhancement factor F defined through Eq. (13) is able to quantify to what extent the field amplitude is enhanced by resonant scattering. In Fig. 7 we plot the enhancement factors for the first ($p = 1$ in Eq. (8)) structural resonance of $BSCs$ 2, 3, 7, and 8 as well as the BCRs used in Fig. 6. The arrays were illuminated with a plane wave with frequency equal to the frequency of the resonance. The k_x - component of the incident wave each time was tuned to the maximum response which in case of BSC were given by Eq. (7). For BCR the maximum response was found at the strict normal incidence. One can see that only for the side-coupled resonances BSC 2,7 the enhancement factor is nicely fit by the expected dependence $F \sim \sqrt{Q} \sim N$ [71]. Notice that in the above reference the enhancement was defined through intensity rather that amplitude. For the edge-coupled resonances we were unable to produce a simple polynomial fit which is probably due to the residual side-coupling emerging through the specific excitation of the resonance by a plane wave. More interesting, though, is that the side-coupled resonances BSC 2,7 produce significantly larger enhancement factors than the edge-coupled ones, and hence

Optics EXPRESS

should be opted for as the operating resonances for light enhancement. In lossy silicon the limits for the enhancement factor of the side-coupled resonances will be placed at the same arrays lengths as were found from Fig. 6 for the Q-factors. Thus, comparing Fig.7 against Fig.6 one can conclude that the amplitude enhancement factors $F \approx 10$–25 can be achieved with arrays of 10–15 silicon subwavelength nanospheres in the red-to-near-infrared range with the side-coupled resonances.

5. Conclusion

We demonstrated that the traces of bound states in the continuum in one-dimensional dielectric arrays can be observed as a specific family of high-Q resonances specified by the number of half-wavelengths placed between the edges of the arrays. Two types of such resonances were identified. The edge-coupled resonances possessing a higher Q-factor are similar to the below continuum resonances known earlier [33] to have the Q-factor scaling law as $Q \sim N^3$ with N being the number of elements in the array. In contract, the side-coupled resonances with lesser Q-factors have the scaling law $Q \sim N^2$. Interestingly, it is the side-coupled resonances related to BSCs that under illumination by a plane wave demonstrate higher enhancement factors providing a platform for light enhancement by finite dielectric arrays with the parameters tuned to a BSC.

It should be pointed out that in terms of both the Q-factor asymptotics and compactness our set-up is no match to ultra-compact Fabry-Perot cavities [80] where the Q-factor scales exponentially with the number of periods in Bragg mirrors. Those asymptotics, however, are hard to achieve in silicon nonophotonics as the subwavelength spheres are scaled down in size to the visible wavelength where the material losses become significant. Our simulations show that in the red-to-near-infrared range the Q-factors of 10^3–10^4 and the amplitude enhancement factors $F \approx 10$–25 can be achieved with arrays of 10–15 silicon subwavelength nanospheres.

In contrast to familiar Fano resonances [56–59] the structural resonances in finite systems are shown to generate a complicated picture in the resonant response to illumination by a plane wave. With the frequency of the impinging wave tuned to the structural resonance we observed the oscillating behavior of the enhanced EM-field amplitude under variation of the wave vector component directed along the array. In real systems the effect of finiteness will be always eventually obscured by material losses. One may expect that with the increase of the length of the array the many pronounced resonances will merge into a Fano feature. We speculate that this picture could be explained by a properly set coupled mode theory [81] based on analytical estimates for resonant frequencies and mode shapes obtained in this paper. Along with asymptotic scaling law for edge-coupled resonances enhancement factor this constitutes a goal for future studies.

The bound states in the continuum were recently employed for engineering high-Q resonators for compact nanophotonic lasers [82] providing access to new coherent sources with intriguing topological properties for optical trapping, biological imaging, and quantum communication. To provide useful guidelines for practical implementations of structures supporting the bound states the effects of both structural fluctuations [83] and substrate coupling [84] have recently been considered. As it was mentioned earlier in the introduction the BSCs are only allowed in infinite systems [72] so that in design of BSC-based devices the researchers will always be bound with residual radiation losses. We believe that our model of the BSC related structural resonances sheds some light onto important aspects of emerging BSC nanophotonics [45, 85].

Funding

Ministry of Education and Science of Russian Federation (state contract N3.1845.2017/4.6) and RFBR grant 16-02-00314.

Acknowledgment

We appreciate discussions with Almas F. Sadreev and Polina N. Semina.